Annealing of Thin "Tincone" Films, a Tin-based Hybrid Material deposited by Molecular Layer Deposition, in Reducing, Inert and Oxidizing Atmospheres

Kevin Van de Kerckhove,* Jolien Dendooven, and Christophe Detavernier

Department of Solid State Sciences, Ghent University, Krijgslaan 281 S1, 9000 Ghent, Belgium

E-mail: kevin.vandekerckhove@ugent.be

Abstract

Molecular layer deposition (MLD) of hybrid organic-inorganic thin films called "tincones" is achieved using tetrakisdimethylaminotin (TDMASn) as the metal precursor, and glycerol (GL) as the organic reactant. The GL-based process displays linear growth and self-limiting surface reactions in a broad temperature window ranging from 75 °C to 200 °C. At higher temperatures no film growth is possible. The GPC decreases rapidly with increasing temperature from 1.3 Å at 75 °C to less than 0.1 Å at 200 °C. The films are observed to be smooth with scanning electron microscopy (SEM) and atomic force microscopy (AFM). The hybrid organic-inorganic nature of the films is visible in both infrared spectroscopy (FTIR) and X-ray photoelectron spectroscopy (XPS). As deposited tincone films are annealed in reducing (H_2), inert (He) or oxidizing (O_2) atmospheres. *In situ* X-ray diffraction (XRD) is employed to study the crystallization of the films during annealing. Tincone films annealed in reducing or inert atmosphere crystallize into a tetragonal SnO phase at 388 °C and 410 °C respectively. These temperatures are lower than the crystallization temperature of 480 °C for ALD tin oxide films annealed in H_2. Tincone films annealed in oxygen crystallize into a SnO_2 phase at a temperature of 523 °C which is similar to the crystallization temperature for ALD tin oxide films annealed in He or O_2. This reduced temperature for crystallization into SnO for the tincone films is interesting since SnO is one of the few metal oxides known as a p-type semiconductor material.

Introduction

The current trend towards miniaturization of electronic devices and components is a driving force for research into the deposition and properties of thin films. One thin-film deposition technique that has gained a significant amount of traction in recent years is atomic layer deposition (ALD). The ALD technique allows the controlled deposition of nanoscale films of a wide variety of materials (including metals, metal oxides, sulfides, etc.) through sequential exposure of the substrate to a precursor and reactant.[1] The self-limiting nature of the gas-surface reactions allow for sub-nanometer thickness control and great conformality on 3D structures.

Molecular layer deposition (MLD) is a thin-film deposition technique closely related to ALD. It is employed for the deposition of purely organic or hybrid organic-inorganic films. The latter is accomplished by combining metal-organic precursors, that are usually well-known from ALD research, with organic reactants such as ethylene glycol (EG) and glycerol (GL). The hybrid films that are deposited by this technique are commonly referred to as "metalcones". An extensive catalog of hybrid materials has already been established in the literature: alucone, titanicone, zincone, zircone, hafnicone, vanadicone, and more.[2–11] To the extent of our knowledge, no MLD process for a tin-based metalcone has been reported yet. Metalcones have been shown to possess several interesting properties in the literature. The organic chains present in the hybrid films add flexibility to the films, which is interesting for applications in flexible electronics and thin-film electrodes.[12,13] Post-deposition treatments are known to transform the metalcone films. Calcination in air and water etching are able to induce porosity in alucone films.[4,14,15] Annealing of metalcone films in inert atmosphere leads to a metal oxide/carbon composite film with improved conductivity.[6,11,16,17]

Tin oxides have a wide variety of technological applications. As a semiconductor with a large band-gap, tin dioxide (SnO_2) is a promising material for solid state gas sensors.[18–20] In optical applications, tin oxides are utilized as a transparent conducting oxide in organic light-emitting diodes (OLED)[21,22] and solar cells[23,24], and as surface coatings for functional glasses, due to their reflectance in the infrared.[25] Tin dioxide is also an interesting, high-capacity, anodic material for lithium-ion batteries.[26–28] Tin monoxide (SnO) is one of the few known p-type semiconductor materials and is hence interesting for electronic applications such as the fabrication of p-n junctions and complementary metal oxide semiconductor (CMOS) architectures.[29,30]

Many ALD processes are known in the literature for the deposition of tin oxide films. $SnCl_4$, SnI_4 and tetrakis-dimethylaminotin (TDMASn) are a few common examples of the Sn metal precursors that are employed in these processes in combination with water, H_2O_2, O_3 or oxygen plasma as the reactant. A nice and thorough overview of tin oxide ALD processes has been written down by Nazorov et al.[31]

In this work, two MLD processes for a novel metalcone material *tincone* were investigated. Both processes employ TDMASn as the tin precursor and ethylene glycol or glycerol as the organic reactant. The growth of the tincone films was monitored *in situ* during the process. The properties of the grown tincone films were characterized with various ex situ methods. A series of as deposited films was subjected to an annealing treatment in reducing (H_2), inert (He) or oxidizing (O_2) atmosphere. The crystallinity of the films was studied during annealing with *in situ* X-ray diffraction.

Experimental

For the deposition of the tincone films, a custom-built, pump-type deposition tool was utilized.[6] The reactor walls were kept at a constant temperature of 130 °C to avoid reactant condensation. The container containing the TDMASn precursor and its delivery line remained at a temperature of 45 °C and 50 °C respectively. Argon (99.999% pure, Air Liquide) was added as a carrier gas to the TDMASn precursor flow in order to increase the exposure of substrate to the precursor. The pressure during TDMASn exposures was 5×10^{-3} mbar. The reactant bubblers of EG and GL remained at a temperature of respectively 80 °C and 60 °C. Similarly as for TDMASn, an additional argon flow was employed during GL exposures. The pressure of EG during the MLD processes was constant at 2×10^{-2} mbar. For GL the pressure was 5×10^{-3} mbar, including the argon carrier gas flow. In between exposures or in idle operation, the base pressure of the reactor vessel was in the 10^{-6} mbar range. Si with native oxide substrates were used for process development, film characterization, and the annealing experiments.

Spectroscopic ellipsometry (SE) was performed with a model M-2000 ellipsometer J.A. Woollam (300 to 1000 nm). SE measurements provide information on the thickness and optical properties of the hybrid films. The included CompleteEASE allowed the analysis of the gathered data. An optical model consisting of a Cauchy dispersion relation was sufficient to accurately describe the SE data. The parameters of the optical model were calibrated with a series of tincone samples with a known thickness from X-ray reflectivity measurements (XRR). The ellipsometer could be mounted on the deposition system. Hence, the growth of the tincone films could be monitored *in situ* by SE.

The morphology of the tincone films was investigated with scanning electron microscopy (SEM) and atomic force microscopy (AFM). SEM imaging was performed on a Quanta 200F (FEI) microscope using a 10 keV electron beam. AFM images were acquired on a Bruker Dimension Edge microscope. The root mean square (rms) roughness was calculated from the measured 1 µm x 1 µm AFM images.

Infrared spectroscopy was carried out on a Vertex 70v Fourier-transform infrared (FTIR) spectrometer from Bruker. A globar source (mid IR), DLaTGS detector and KBr beamsplitter were mounted on the optics bench. The spectrometer remained under vacuum during measurements to avoid the appearance of atmospheric absorptions (mainly CO_2 and H_2O) in the absorption spectra.

X-ray photoelectron spectroscopy (XPS) measurements were executed on a Thermo Scientific Theta Probe system. Aluminium Kα radiation ($\lambda = 0.834$ nm) was used as an excitation source. Analysis of the gathered data was performed in the CasaXPS software.

XRR and X-ray diffraction (XRD) measurements were completed on a Bruker D8 Discover diffractometer. For both XRR and XRD, copper Kα ($\lambda = 0.154$ nm) radiation was utilized. During annealing under reducing (He with 5% H_2), inert (He) or oxidizing (He with 5% O_2) atmospheres, in situ XRD was carried out on a home-built setup fitted with a position-sensitive detector with a range of 20° in 2θ.[32]

Results and discussion

In the first section, the process development and characterization is discussed. Secondly, the results of the annealing experiments of tincone films in reducing, inert and oxidizing atmospheres are presented.

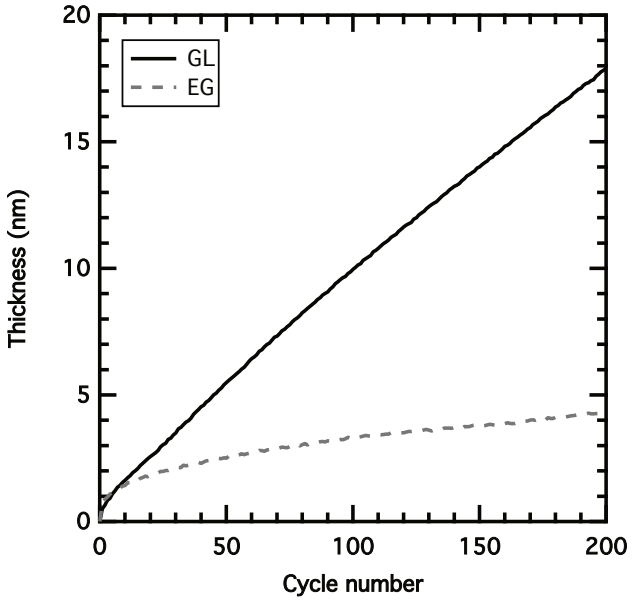

Figure 1: Comparison of the first 200 MLD cycles of the TDMASn/GL and TDMASn/EG processes at a sample temperature of 100 °C.

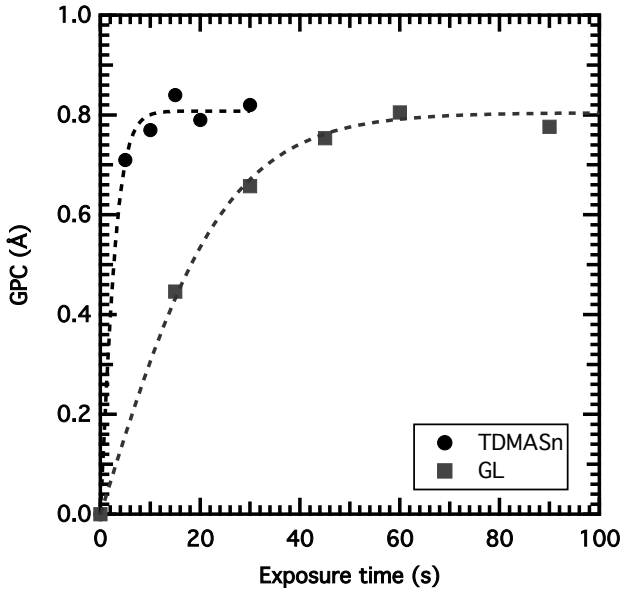

Figure 2: Growth per cycle as a function of precursor and reactant exposure time for the TDMASn/GL MLD process at a sample temperature of 100 °C. Saturation is achieved at exposure times of 20 and 60 seconds for TDMASn and GL respectively.

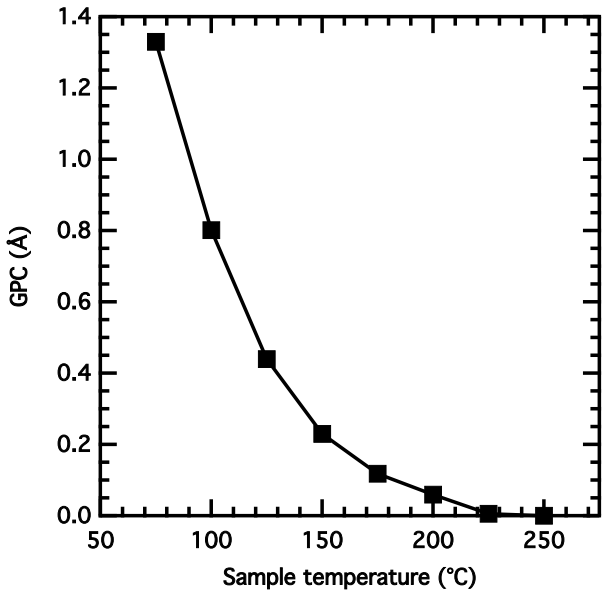

Figure 3: Growth rate versus sample temperature for the TDMASn/GL process. No growth was observed for temperatures above 200 °C.

The tincone MLD process

Process development

In order to develop a MLD process for a tin-based, hybrid film, a suitable inorganic precursor and organic reactant need to be selected. As the inorganic precursor, tetrakis-dimethylaminotin (TDMASn) is chosen since it is known as an ALD precursor for the deposition of SnO_2.[31,33,34] As the organic reactant, ethylene glycol (EG) and glycerol (GL) are tested as they have both been implemented successfully in multiple MLD processes.[2–6,11] By default, the exposure time for TDMASn is 20 s. For EG and GL, the standard pulse times are 30 s and 60 s respectively.

In situ ellipsometry enables the monitoring of the film growth during the TDMASn/EG and TDMASn/GL MLD processes. After every MLD cycle, the film thickness is measured. The results are presented in figure 1. There is a clear difference in the growth curves for both processes. For the TDMASn/GL process, the growth per cycle (GPC) appears to be stable and the film growth is linear over 200 cycles. The GPC is 0.8 Å at a sample temperature of 100 °C. On the other hand, the GPC of the TDMASn/EG process decreases dramatically over the first 50 cycles after which it becomes stable. At a sample temperature of 100 °C, the GPC for the TDMASn/EG process is 0.1 Å after an initial 50 cycles. The decrease in GPC and slower film growth for an EG-based process in combination with an alkylamine metal precursor has been observed before.[6,11] The hypothesis is that both OH end groups of the EG molecules are able to react with surface groups. These double reactions remove active surface sites without adding new groups for the TDMASn molecules to react with. This phenomenon effectively decreases the growth rate of the hybrid film. Previous investigations on alucone films have shown that the inherent flexibility of the organic chains allows these double reactions to proceed, and that these reactions are detrimental for the formation of a smooth and closed film. For the TDMASn/GL process, these possible double reactions do not pose a problem for continued film growth since GL possesses an additional hydroxyl group compared to EG. Due to its low growth rate, the TDMASn/EG process was not

investigated further in this work.

Saturation curves of the GPC were measured to demonstrate the self-limiting nature of the TDMASn/GL process. The saturation curves were measured at sample temperatures of 100 °C (figure 2) and 150 °C. At both temperatures, the GPC saturates at TDMASn and GL exposure times of respectively 20 s and 60 s.

The temperature window for linear film growth with the TDMASn/GL process ranges from 75 to 200 °C. The GPC decreases rapidly with increasing temperature and drops to zero at temperatures above 200 °C. The lower temperature of the temperature window is limited by the temperature of the hot-wall reactor. At the higher end, the sample temperature is not limited due to the high decomposition temperature of TDMASn of 325 °C.[31] An increased TDMASn desorption rate at higher temperatures may explain the decrease in GPC.

Characterization of as deposited films

The composition, morphology, and other properties of as deposited tincone films were studied *ex situ*. The tincone films are grown with 300 cycles of the TDMASn/GL process at a substrate temperature of 100 °C on a silicon substrate with native oxide. All tincone samples used for characterization or annealing experiments were freshly deposited in order to avoid any effect of aging in atmospheric conditions. Although, in the course of a week, no changes in density or composition of the films was observed during aging.

As deposited, the thickness of the films is 28.3 nm and the density is 2.5 g/cm^3. These values were derived from a simulation of the XRR pattern that is in good agreement with the measurement data (figure 4). The surface morphology of the film was verified with AFM. A measurement of an as deposited film is presented in the inset of figure 4 and shows that the films have a low surface roughness. SEM confirms this statement on the nanoscopic level as shown in figure 8.

A working optical model for analyzing the *in situ* ellipsometry data was constructed for the hybrid tincone films. A model consisting of a simple Cauchy dispersion relation of the type $n(\lambda) = A + B/\lambda^2 + C/\lambda^4$ was sufficient for acquiring a good fit for the SE data. A series of tincone film thickness measurements by XRR were employed to calibrate the parameters of the optical model. This calibration procedure yielded the following parameter values: A = 1.408, B = 1.725×10^4 nm^2 and C = -4.29×10^8 nm^4. At a wavelength of 600 nm, the calculated refractive index is 1.45 in this model.

Fourier transform infrared spectroscopy (FTIR) was performed on as deposited tincone films in order to investigate the chemical composition of the films. The films were measured *ex situ*. The result of the measurement is shown in figure 5. Two absorption peaks are visible at 2945 cm^{-1} and 2875 cm^{-1}. These peaks are related to the asymmetrical and symmetrical CH_2 stretch modes respectively. The "fingerprint" region of the spectrum reveals the CH_2 twisting, and C-C and C-O stretching modes at wavenumbers of 1252 cm^{-1}, 1140 cm^{-1} and 1075 cm^{-1} respectively.[2] At lower wavenumbers several tin-related modes appear in the spectrum. The peaks at 960 cm^{-1} and 745 cm^{-1} originate from Sn-O stretching vibrations. The absorption at 870 cm^{-1} has been previously assigned to vibrations of Sn-OH bonds.[35–37] The presence of both inorganic and organic components in the spectrum are indicative of the hybrid nature of the film.

X-ray photoelectron spectroscopy (XPS) was also employed to verify the composition of the films, and the oxidation state of Sn inside the films. For determining the atomic composition of the films, first carbon contamination of the surface was removed with two argon sputtering steps. This ensures that the measured carbon signal orig-

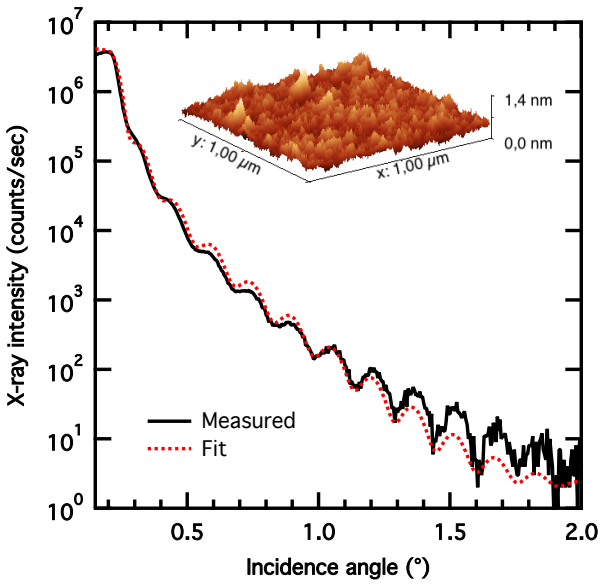

Figure 4: X-ray reflectivity measurement of a tincone film, deposited with 300 TDMASn/GL MLD cycles and the simulated data fit for determining the film thickness and density. The inset shows an 1 µm by 1 µm AFM image of the same film, illustrating its low rms surface roughness of 0.18 nm.

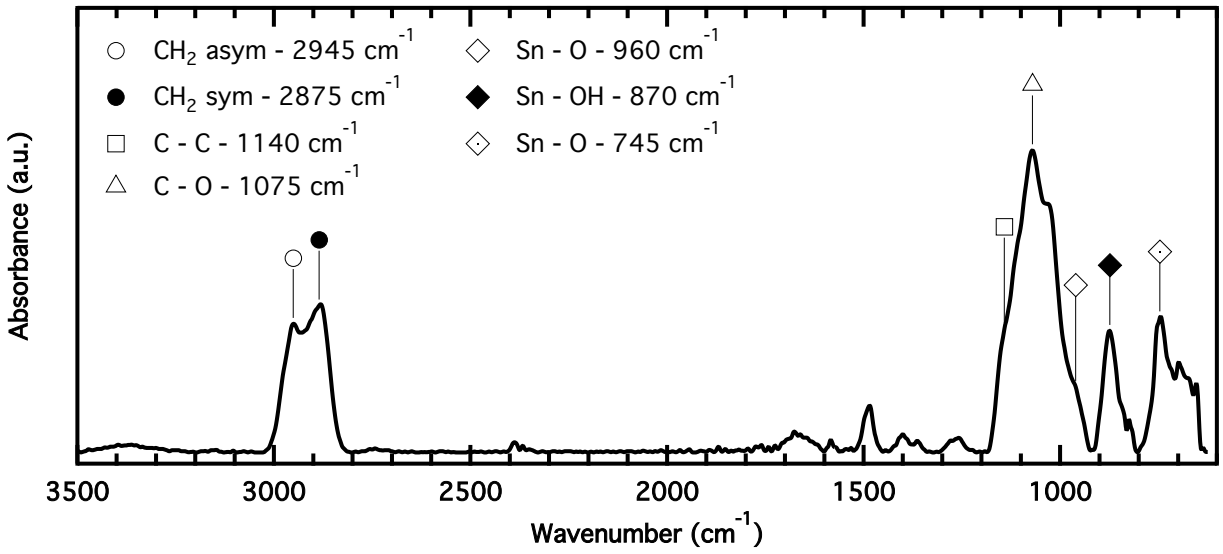

Figure 5: Infrared spectrum of a 28 nm tincone film, deposited with 300 cycles of the TDMASn/GL MLD process.

inates from inside the hybrid film, and not from a contaminated surface. The result of the composition analysis can be seen in table 2. The as deposited film contains about 15 at% of carbon. Nitrogen contamination from the TDMASn precursor is not observed. The oxidation state of tin inside the hybrid film is determined from the surface XPS spectra, which are calibrated by the carbon 1s line at 284.4 eV. In figure 9, the $3d_{3/2}$ and $3d_{5/2}$ lines of the spectra can be seen. For the as deposited film, the $3d_{3/2}$ and $3d_{5/2}$ lines are centered around 494.6 eV and 486.0 eV respectively, which is indicative of the Sn^{2+} oxidation state. This is unexpected since the oxidation state of tin in the TDMASn precursor is 4+.

Annealing in reducing, inert and oxidizing atmospheres

A series of tincone and SnO_2 (deposited by ALD) films were annealed in reducing (He with 5% H_2), inert (He) and oxidizing (atmospheres He with 5% O_2) at temperatures up to 700 °C. The films were heated at a ramp rate of 10 °C/min. After reaching the highest temperature of the treatment, the temperature was kept constant for 10 min before turning off the heating.

The hybrid tincone films were deposited by executing 300 cycles of the TDMASn/GL MLD process at 100 °C on a silicon substrate with native oxide. The thickness of the films was 28 nm as deposited. The purely inorganic SnO_2 films were deposited by the TDMASn/H_2O ALD process.[34] The substrate temperature during deposition was also 100 °C and 500 cycles in total were executed. After deposition, the film thickness was measured to be 45 nm with XRR. The same substrate was used as for the tincone films.

During the annealing treatments, the crystallinity of the films was monitored via *in situ* X-ray diffraction (XRD). A detection range in 2θ from 23° to 42° was chosen since the most prominent SnO and SnO_2 reflections are expected to appear in this range. After the treatment, the morphology of the films was verified with SEM, and the composition and tin oxidation state with XPS.

An overview of the *in situ* XRD measurements during the annealing of the tincone films is presented in figure 6 and the results are summarized in table 1. During annealing in H_2 and He, a single, strong diffraction peak appears at 36.7°. This peak is assigned to the (0 0 2) lattice plane of the tetragonal SnO phase (Romarchite, ICSD card no. 015516). For the anneal in reducing atmosphere, the onset of crystallization is observed at a temperature of 388 °C. At a temperature of 600 °C, the phase disappears again. This is probably due to a further reduction of SnO into metallic Sn, which then evaporates from the surface. In inert atmosphere, crystallization starts at 410 °C. An anneal in oxidizing atmosphere results in the appearance of a tetragonal SnO_2 phase. Two main diffraction peaks are observed at 26.5° and 37.9°. These peaks correspond to the (1 1 0) and (2 0 0) orientations respectively (ICSD card no. 084576). This phase is formed at temperatures above 523 °C.

The heat treatments listed above were repeated on ALD SnO_2 films. The results of *in situ* XRD during annealing are shown in figure 7 and table 1. In reducing atmosphere, the as deposited amorphous SnO_2 film is reduced and crystallizes into a tetragonal SnO phase (Romarchite, ICSD card no. 015516). Three reflections are observed at 29.5°, 32.7°, and 36.7° that originate from the (1 0 1), (1 1 0) and (0 0 2) orientations respectively. The onset of crystallization is observed at a temperature of 480 °C. Annealing of the ALD SnO_2 films in He and O_2 results in the tetragonal SnO_2 phase (ICSD card no. 084576). At temperatures above 545 °C, three peaks are observed in the diffractogram. The peaks are located at 26.5°, 34.1°, and 38.0°. They are attributed to the (1 1 0), (1 0 1), and

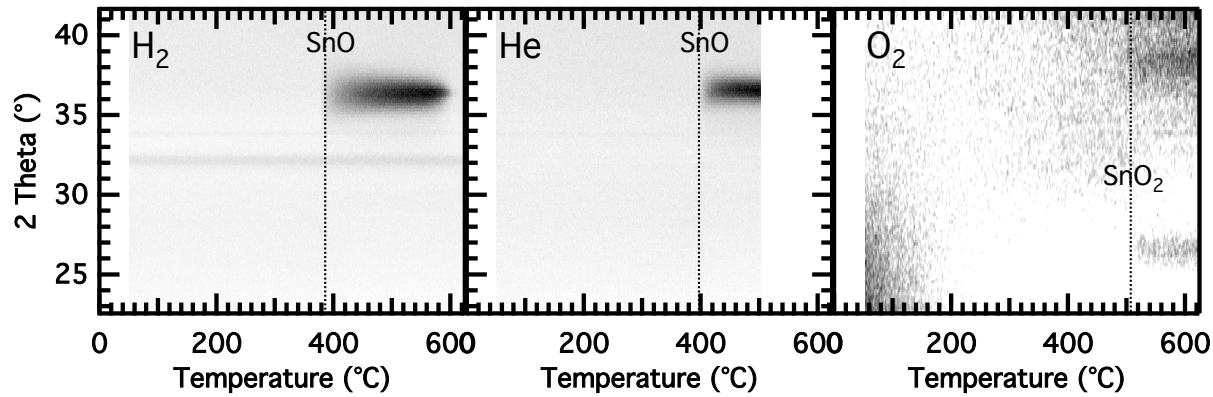

Figure 6: *In situ* XRD measurements during annealing of tincone films, deposited with 300 MLD cycles, in reducing (H_2), inert (He), and oxidizing (O_2) atmospheres. The films were heated at a rate of 10 °C/min to 700 °C, 500 °C, and 700 °C in each atmosphere respectively.

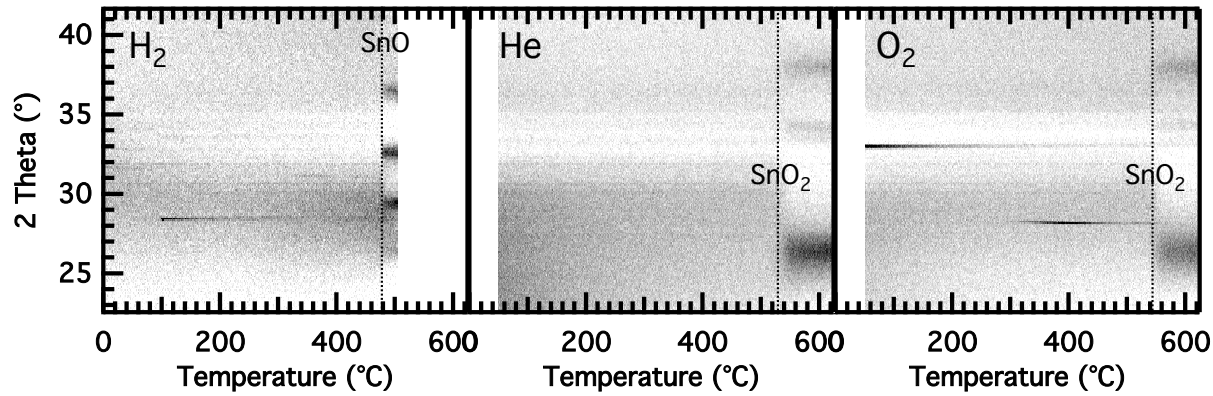

Figure 7: *In situ* XRD measurements during annealing of reference SnO_2 films of 45 nm, deposited by the TDMASn/H_2O, in reducing (H_2), inert (He), and oxidizing (O_2) atmospheres. The films were heated at a rate of 10 °C/min to 500 °C, 700 °C and 700 °C in each atmosphere respectively.

Table 1: Overview table of the formation temperatures (top) and phases (bottom) during annealing of as deposited MLD tincone and ALD SnO_2 in reducing (H_2), inert (He), and oxidizing (O_2) atmospheres.

	H_2	He	O_2
Tincone	388 °C SnO (tetragonal)	410 °C SnO (tetragonal)	523 °C SnO_2 (tetragonal)
ALD SnO_2	480 °C SnO (tetragonal)	545 °C SnO_2 (tetragonal)	545 °C SnO_2 (tetragonal)

(2 0 0) lattice planes respectively.

After annealing, the morphology of the films is investigated via SEM imaging. Representative images of the films are shown in figure 8. The samples annealed in hydrogen and helium display a rough surface and a grainy structure that was formed during crystallization. Small agglomerated islands are visible in the samples annealed in oxygen.

The tin oxidation state and composition of the annealed films were determined with XPS. The $3d_{3/2}$ and $3d_{5/2}$ lines of the XPS spectra are presented in figure 9. The position of these lines with respect to a calibrated carbon 1s line provides information about the oxidation state of tin inside the films. For the samples annealed in H_2 and He, the $3d_{3/2}$ and $3d_{5/2}$ lines are centered around 494.6 eV and 486.0 eV respectively. This suggests a 2+ oxidation state of tin for these samples. The XPS spectrum of the samples annealed in oxygen shows that the $3d_{3/2}$ and $3d_{5/2}$ lines are located at 495.2 eV and 486.7 eV and implies a Sn^{4+} state. This observation is in line with the tin oxide phases observed in *in situ* XRD. The composition analysis with XPS of the annealed films is presented in table 2. The heat treatment significantly reduces the carbon content of the films. The measured stoichiometry of the films also coincides with the observed phases.

Comparison of the *in situ* XRD results of the tincone and ALD SnO_2 films show several notable differences. The first main difference is crystallization behaviour of the films in inert atmosphere. The tincone films crystallize into the SnO phase, while the ALD SnO_2 crystallize, unsurprisingly, into the SnO_2. This can be explained by considering the starting oxidation state of tin in the as deposited films. For the tincone films tin can be found in the Sn^{2+} state as opposed to the ALD films where tin is in the Sn^{4+} state. Secondly, the SnO phase formation in the tincone films shows only a single, strong reflection while the SnO phase in the ALD films shows multiple. Hence, the tincone SnO phase is preferentially oriented towards the (0 0 2) lattice plane. A final important difference is the crystallization temperature of the SnO phase. This temperature is generally lower for the tincone samples, as is illustrated in figure 10. For films annealed in hydrogen, the onset temperature for crystallization is approximately 90 °C lower for the tincone films as compared to the ALD films. The crystallization temperature for tincone annealed in He is about 70 °C lower with respect to the H_2-annealed ALD films. The SnO_2 phase crystallization temperature is, however, similar for both tincone and ALD SnO_2 films.

Conclusions

In this work, the growth and properties of hybrid, tin-based *tincone* films, deposited by molecular layer deposition, was investigated. For the deposition process, tetrakisdimethylaminotin (TDMASn) was employed as the metallorganic precursor for tin in combination with ethylene glycol (EG) and glycerol (GL) as the organic reactants. Steady-state growth was achieved for both processes. The growth per cycle (GPC) for the TDMASn/EG process was, however, considerably lower (0.1 Å at 100 °C) than for the TDMASn/GL process (0.8 Å at 100 °C). For this reason, only the TDMASn/GL process was studied further in this work. The TDMASn/GL process displayed linear and saturated growth in a broad temperature range. With increasing temperature, the growth per cycle decreased rapidly from 1.3 Å at 75 °C to less than 0.1 Å at 200 °C. No growth was observed at higher temperatures.

The refractive index and density of the as deposited films were determined to be 1.45 at 600 nm and 2.5 g/cm^3 with SE and XRR respectively. The morphology of the films

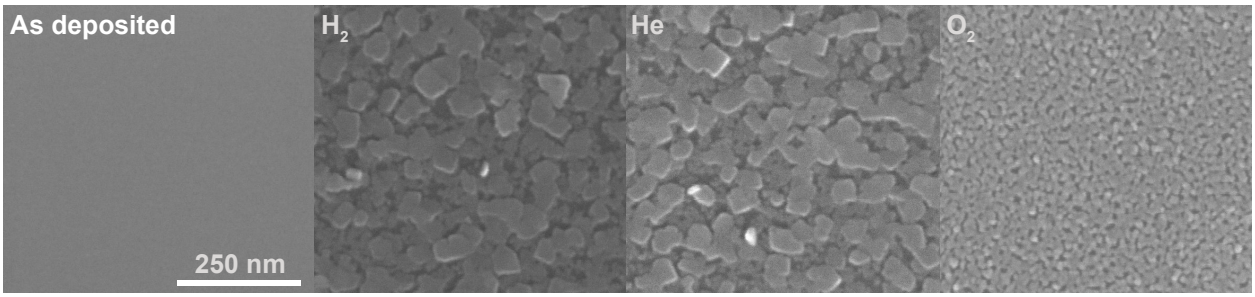

Figure 8: SEM images of the as deposited and annealed tincone samples. The samples annealed in H_2 and He were quenched at 500 °C. The samples annealed in O_2 were quenched at 700

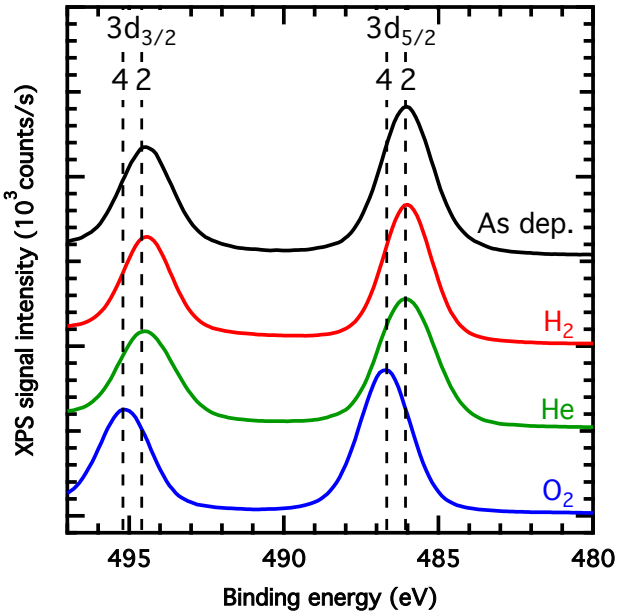

Figure 9: Difference in tin oxidation state between the different tincone samples, as measured by XPS. The carbon 1s line was calibrated at 284.8 eV. The samples annealed in H_2 and He were quenched at 500 °C.

Table 2: Summary of the characterization results of the as deposited and annealed tincone films. The samples annealed in H_2 and He were quenched at 500 °C.

	Crystallinity	Composition (at%)		
		C	Sn	O
As deposited	Amorphous	15	52	33
Anneal in He to 500 °C	SnO	5	52	43
Anneal in H_2 to 500 °C	SnO	7	53	40
Anneal in O_2 to 700 °C	SnO_2	1	38	61

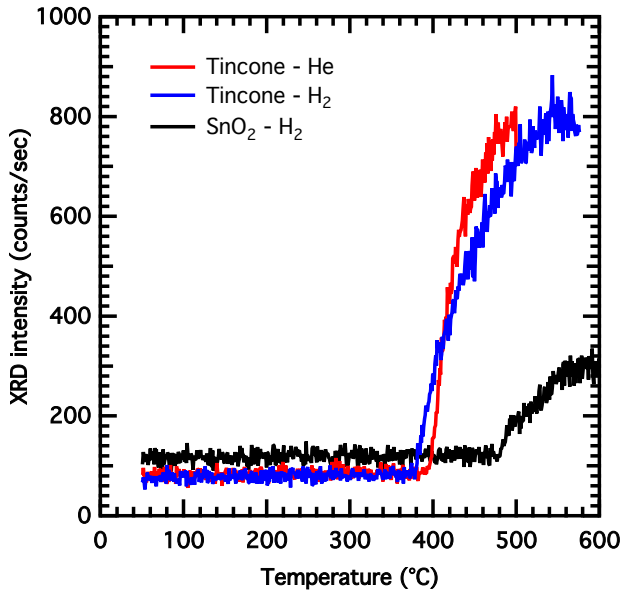

Figure 10: XRD intensity of the (2 0 0) SnO reflection as a function of temperature. The (2 0 0) reflection corresponds to a 2θ value of 36.7 degrees.

was shown to be smooth with a low surface roughness with SEM and AFM. The hybrid nature of the as deposited films was confirmed with both FTIR and XPS. Both spectra displayed both organic and inorganic components. XPS revealed the oxidation state of tin in the as deposited films to be 2+.

As deposited tincone films were annealed in reducing (H_2), inert (He) or oxidizing (O_2) atmospheres. The crystallization of the films was studied *in situ* with X-ray diffraction (XRD). *Ex situ* the annealed films were studied with SEM and XPS. For comparison purposes, tin oxide films deposited via ALD were subjected to identical annealing treatments. XRD revealed that both the films annealed in reducing or inert atmospheres crystallized to a tetragonal tin monoxide phase at 388 °C and 410 °C respectively. This was supported by XPS measurements that indicated a 2+ oxidation state for tin. In comparison, the ALD tin oxide films crystallized into SnO only in reducing atmosphere and at a higher temperature of 480 °C. The tincone films that crystallized into SnO during annealing displayed a grainy and rough structure in SEM, and a significantly reduced carbon content in XPS. The tincone films annealed in oxygen crystallized into a tetragonal SnO_2 phase at 523 °C. This observation was also supported by a tin oxidation state of 4+ seen in XPS. Similar crystallization behaviour was observed for

the reference ALD tin oxide films that were annealed in inert or oxidizing atmosphere. Tincone films annealed in oxygen showed small agglomerated islands in SEM. XPS indicated that all carbon content was removed from these films during the annealing treatment.

This work adds a new hybrid "metalcone" to the catalog of materials that can be deposited via MLD. The results from the annealing experiments may prove to be interesting for the semiconductor industry since SnO is one of the few metal oxides known as a p-type semiconductor material.

Acknowledgement

The authors are grateful to FWO Vlaanderen for providing Kevin Van de Kerckhove with financial support through the mandate of Aspirant. J.D. acknowledges the FWO for a post-doc grant. They also acknowledge the IWT Vlaanderen (IWT-SBO SOSLion project), BOF-UGent (GOA 01G01513), and the Hercules foundation for providing funding for this work. They thank Karl Opsomer and Matthias Minjauw for the XPS measurements, Tareq Ahmad for AFM, and Olivier Janssens for SEM work.

References

(1) George, S. M. *Chemical Reviews* **2010**, *110*, 111–131.

(2) Bertrand, J. A.; Dameron, A. A.; Seghete, D.; Burton, B. B.; Davidson, S. D.; Cavanagh, A. S.; George, S. M. *Chemistry of Materials* **2008**, *20*, 3315–3326.

(3) George, S. M.; Lee, B. H.; Yoon, B.; Abdulagatov, A. I.; Hall, R. A. *Journal of Nanoscience and Nanotechnology* **2011**, *11*, 7948–7955.

(4) Van de Kerckhove, K.; Barr, M. K. S.; Santinacci, L.; Vereecken, P. M.; Dendooven, J.; Detavernier, C. *Dalton Transactions* **2018**,

(5) Abdulagatov, A. I.; Hall, R. A.; Sutherland, J. L.; Lee, B. H.; Cavanagh, A. S.; George, S. M. *Chemistry of Materials* **2012**, *24*, 2854–2863.

(6) Van de Kerckhove, K.; Mattelaer, F.; Deduytsche, D.; Vereecken, P. M.; Dendooven, J.; Detavernier, C. *Dalton Transactions* **2016**, *45*, 1176–1184.

(7) Yoon, B.; O'Patchen, J. L.; Seghete, D.; Cavanagh, A. S.; George, S. M. *Chemical Vapor Deposition* **2009**, *15*, 112–121.

(8) Peng, Q.; Gong, B.; VanGundy, R. M.; Parsons, G. N. *Chemistry of Materials* **2009**, *21*, 820–830.

(9) Lee, B. H.; Anderson, V. R.; George, S. M. *Chemical Vapor Deposition* **2013**, *19*, 204–212.

(10) Lee, B. H.; Anderson, V. R.; George, S. M. *ACS Applied Materials & Interfaces* **2014**, *6*, 16880–16887.

(11) Van de Kerckhove, K.; Mattelaer, F.; Dendooven, J.; Detavernier, C. *Dalton Transactions* **2017**, *192*, 1126–20.

(12) Lee, B. H.; Lee, K. H.; Im, S.; Sung, M. M. *Organic Electronics* **2008**, *9*, 1146–1153.

(13) Lee, B. H.; Yoon, B.; Anderson, V. R.; George, S. M. *The Journal of Physical Chemistry C* **2012**, *116*, 3250–3257.

(14) Liang, X.; Yu, M.; Li, J.; Jiang, Y.-B.; Weimer, A. W. *Chemical Communications* **2009**, 7140–7142.

(15) Liang, X.; Evanko, B. W.; Izar, A.; King, D. M.; Jiang, Y.-B.; Weimer, A. W. *Microporous and Mesoporous Materials* **2013**, *168*, 178–182.

(16) DuMont, J. W.; George, S. M. *Journal of Physical Chemistry C* **2015**, *119*, 14603–14612.

(17) Abdulagatov, A. I.; Terauds, K. E.; Travis, J. J.; Cavanagh, A. S.; Raj, R.; George, S. M. *Journal of Physical Chemistry C* **2013**, *117*, 17442–17450.

(18) Rumyantseva, M. N.; Safonova, O. V.; Boulova, M. N.; Ryabova, L. I.; Gas'kov, A. M. *Russian Chemical Bulletin* **2003**, *52*, 1217–1238.

(19) Arafat, M. M.; Dinan, B.; Akbar, S. A.; Haseeb, A. S. M. A. *Sensors* **2012**, *12*, 7207–7258.

(20) Choi, G.; Satyanarayana, L.; Park, J. *Applied Surface Science* **2006**, *252*, 7878–7883.

(21) Tan, S.-S.; Kee, Y.-Y.; Wong, H.-Y.; Tou, T.-Y. *Surface & Coatings Technology* **2013**, *231*, 98–101.

(22) Görrn, P.; Ghaffari, F.; Riedl, T.; Kowalsky, W. *Solid State Electronics* **2009**, *53*, 329–331.

(23) Chou, L.-W.; Lin, Y.-Y.; Wu, A. T. *Applied Surface Science* **2013**, *277*, 30–34.

(24) Kang, B.; Tan, L. W.; Silva, S. R. P. *Applied Physics Letters* **2008**, *93*, 133302–3.

(25) Gordon, R. *Journal of Non-Crystalline Solids* **1997**, *218*, 81–91.

(26) Idota, Y. *Science* **1997**, *276*, 1395–1397.

(27) Mohamedi, M.; Lee, S. J.; Takahashi, D.; Nishizawa, M.; Itoh, T.; Uchida, I. *Electrochimica Acta* **2001**, *46*, 1161–1168.

(28) Meduri, P.; Pendyala, C.; Kumar, V.; Sumanasekera, G. U.; Sunkara, M. K. *Nano Letters* **2009**, *9*, 612–616.

(29) Caraveo-Frescas, J. A.; Nayak, P. K.; Al-Jawhari, H. A.; Granato, D. B.; Schwingenschlögl, U.; Alshareef, H. N. *ACS Nano* **2013**, *7*, 5160–5167.

(30) Han, J. H.; Chung, Y. J.; Park, B. K.; Kim, S. K.; Kim, H.-S.; Kim, C. G.; Chung, T.-M. *Chemistry of Materials* **2014**, *26*, 6088–6091.

(31) Nazarov, D. V.; Bobrysheva, N. P.; Osmolovskaya, O. M.; Osmolovsky, M. G.; Smirnov, V. M. *Reviews on Advanced Materials Science* **2015**, *40*, 262–275.

(32) Knaepen, W.; Detavernier, C.; Van Meirhaeghe, R. L.; Jordan Sweet, J.; Lavoie, C. *Thin Solid Films* **2008**, *516*, 4946–4952.

(33) Elam, J. W.; Baker, D. A.; Hryn, A. J.; Martinson, A. B. F.; Pellin, M. J.; Hupp, J. T. *Journal of Vacuum Science & Technology A* **2008**, *26*, 244–252.

(34) Mullings, M. N.; Hägglund, C.; Bent, S. F. *Journal of Vacuum Science & Technology A* **2013**, *31*, 061503–9.

(35) Chaisitsak, S. *Sensors* **2011**, *11*, 7127–7140.

(36) Van Tran, T.; Turrell, S.; Eddafi, M.; Capoen, B.; Bouazaoui, M.; Roussel, P.; Berneschi, S.; Righini, G.; Ferrari, M.; Bhaktha, S. N. B.; Cristini, O.; Kinowski, C. *Journal of Molecular Structure* **2010**, *976*, 314–319.

(37) Khan, A. F.; Mehmood, M.; Aslam, M.; Ashraf, M. *Applied Surface Science* **2010**, *256*, 2252–2258.

Graphical TOC Entry